J|A|C|S ARTICLES

Published on Web 03/04/2010

Photoelectrochemical Water Oxidation by Cobalt Catalyst ("Co−Pi")/α-Fe_2O_3 Composite Photoanodes: Oxygen Evolution and Resolution of a Kinetic Bottleneck

Diane K. Zhong and Daniel R. Gamelin*

Department of Chemistry, University of Washington, Seattle, Washington 98195-1700

Received October 13, 2009; E-mail: Gamelin@chem.washington.edu

Abstract: A cobalt−phosphate water oxidation catalyst ("Co−Pi") has been electrodeposited onto mesostructured α-Fe_2O_3 photoanodes. The photoelectrochemical properties of the resulting composite photoanodes were optimized for solar water oxidation under frontside illumination in pH 8 electrolytes. A kinetic bottleneck limiting the performance of such photoanodes was identified and shown to be largely overcome by more sparse deposition of Co−Pi onto the α-Fe_2O_3. Relative to α-Fe_2O_3 photoanodes, a sustained 5-fold enhancement in the photocurrent density and O_2 evolution rate was observed at +1.0 V vs RHE with the Co−Pi/α-Fe_2O_3 composite photoanodes. These results demonstrate that integration of this promising water oxidation catalyst with a photon-absorbing substrate can provide a substantial reduction in the external power needed to drive the catalyst's electrolysis chemistry.

I. Introduction

Photoelectrochemical (PEC) water splitting has been envisioned as a promising strategy for collecting the energy of sunlight and storing it in the form of chemical bonds.[1−5] Water splitting is complicated by its multielectron nature (eqs 1 and 2). The more challenging of these two processes, water oxidation (eq 1), requires removal of a total of four electrons and four protons from two water molecules to form one O_2 molecule.

$$2H_2O \rightarrow O_2 + 4H^+ + 4e^- \quad (1)$$

$$4H^+ + 4e^- \rightarrow 2H_2 \quad (2)$$

Solar PEC water splitting has been explored extensively but is still hindered by the major challenge of identifying photoelectrode materials that are simultaneously inexpensive, efficient, and stable under reaction conditions.[5−7] Much of this challenge ultimately derives from the fact that materials optimized for photon absorption and charge separation are not generally also optimized for catalysis or stability and vice versa. For example, in PEC cells, photon absorption and water oxidation are typically performed by the same photoanode material (e.g., α-Fe_2O_3, WO_3, N:TiO_2) that has been optimized globally for PEC performance, balancing the needs for photon absorption and charge separation against the demands of stability and catalytic competence. This compromise usually results in the need for high overpotentials to achieve large current densities, limiting the efficiency of this approach for solar energy conversion.

Solar-powered bulk electrolysis allows separation of the tasks of photon absorption and catalysis and allows optimization of the photon absorption and water splitting functions independently. This is the strategy implemented in biology, where water oxidation is catalyzed by the Mn_4O_xCa cluster of photosystem II (PS II) at low overpotentials,[8,9] with the overpotentials ultimately supplied by solar photons absorbed elsewhere by light-harvesting antennae. Substantial research has been directed at developing several attractive synthetic water oxidation electrocatalysts that can operate at low overpotentials,[10−12] but such electrocatalysts frequently contain expensive metals (Ru, Ir) or require extreme pH conditions. Recently, an amorphous cobalt−phosphate-based material, referred to here as "Co−Pi", was discovered that catalyzes water oxidation at relatively low overpotentials in pH 7 phosphate buffer.[13−15] Co−Pi is fabricated on transparent conducting oxide substrates by a simple electrodeposition method from solutions containing 0.5 mM Co^{2+} and 0.1 M potassium phosphate buffered at pH 7. The active catalyst is believed to have a cubane structure loosely resembling the oxygen-evolving complex of PS II.[16−18] Consist-

(1) Heller, A. *Science* **1984**, *223*, 1141–1148.
(2) Grätzel, M. *Nature* **2001**, *414*, 338–344.
(3) Lewis, N. S.; Nocera, D. G. *Proc. Natl. Acad. Sci.* **2006**, *103*, 15729–15735.
(4) Lewis, N. S. *Science* **2007**, *315*, 798–801.
(5) Grimes, C.; Varghese, O. K.; Ranjan, S. *Light, Water, Hydrogen*; Springer: New York, 2007.
(6) Woodhouse, M.; Parkinson, B. A. *Chem. Mater.* **2008**, *20*, 2495–2502.
(7) Kudo, A.; Miseki, Y. *Chem. Soc. Rev.* **2009**, *38*, 253–278.
(8) McEvoy, J. P.; Brudvig, G. W. *Chem. Rev.* **2006**, *106*, 4455–4483.
(9) Barber, J.; Murray, J. W. *Coord. Chem. Rev.* **2008**, *252*, 233–243.
(10) Tseng, H.-W.; Zong, R.; Muckerman, J. T.; Thummel, R. *Inorg. Chem.* **2008**, *47*, 11763–11773.
(11) McDaniel, N. D.; Coughlin, F. J.; Tinker, L. L.; Bernhard, S. J. *J. Am. Chem. Soc.* **2008**, *130*, 210–217.
(12) Romero, I.; Rodríguez, M.; Sens, C.; Mola, J.; Kollipara, M. R.; Francàs, L.; Mas-Marza, E.; Escriche, L.; Llobet, A. *Inorg. Chem.* **2008**, *47*, 1824–1834.
(13) Kanan, M. W.; Nocera, D. G. *Science* **2008**, *321*, 1072–1075.
(14) Surendranath, Y.; Dincă, M.; Nocera, D. G. *J. Am. Chem. Soc.* **2009**, *131*, 2615–2620.
(15) Lutterman, D. A.; Surendranath, Y.; Nocera, D. G. *J. Am. Chem. Soc.* **2009**, *131*, 3838–3839.
(16) Risch, M.; Khare, V.; Zaharieva, I.; Gerencser, L.; Chernev, P.; Dau, H. *J. Am. Chem. Soc.* **2009**, *131*, 6936–6937.

10.1021/ja908730h

ing of earth-abundant elements cobalt, potassium, and phosphorus in a ca. 2:1:1 ratio, Co−Pi meets many of the general criteria for widely distributed electrolysis applications.[18,19] To drive this catalyst, a bias of >∼1.51 V vs RHE is needed, and current densities of 1.2 mA/cm^2 are reached at approximately +1.7 V vs RHE in pH 7 phosphate buffer (the sum of the thermodynamic potential for water oxidation and the overpotential required to reach 1.2 mA/cm^2 (+1.23 and ∼+0.5 V vs RHE, respectively)).[13] The external power required to drive this electrocatalyst is ultimately envisioned as coming from solar photovoltaics or other renewables.[19,20] If some or all of the need for this external power could be eliminated by directly powering the catalyst using a light-harvesting semiconductor substrate (instead of transparent conducting oxides), this approach to solar energy storage could become even more attractive.

As proof of concept, photoelectrolysis by composite photoanodes prepared by deposition of Co−Pi onto the cheap and abundant photoanode material α-Fe_2O_3 was demonstrated recently.[21] It was found that light can supply some of the energy needed to drive water oxidation by Co−Pi in this integrated composite structure, but operation was only demonstrated under caustic conditions (pH > 13), making this system nonideal.[20] Sustained solar water oxidation by Co−Pi/α-Fe_2O_3 composite photoanodes at lower pH levels remains to be demonstrated. Additionally, improvement of overall efficiencies could be expected from optimization of these photoanodes for frontside illumination, but this was not demonstrated previously.

Here, we report three major improvements of these composite photoanodes: (i) Nonproductive photon absorption by the catalyst has been diminished sufficiently to allow frontside illumination, yielding an ∼200% enhancement of efficiency at +1.0 V vs RHE relative to the previous report, (ii) sustained operation in buffered salt water at pH 8 has been demonstrated, and (iii) sustained O_2 evolution with a ∼500% enhancement over the parent α-Fe_2O_3 photoanodes has been demonstrated at +1.0 V vs RHE. By combining Co−Pi with α-Fe_2O_3 photoanodes, the external bias needed to drive water oxidation by this catalyst at 1 mA/cm^2 has been decreased by more than 0.5 V under 1 sun, AM 1.5 solar irradiation.

II. Experimental Section

A. Fabrication of α-Fe_2O_3 Photoanodes. Si-doped α-Fe_2O_3 photoanodes were fabricated on fluorine-doped tin oxide (FTO) glass (50 × 13 × 2.3 mm TEC 15 Hartford Glass Co.) at 470 °C for 5 min by atmospheric pressure chemical vapor deposition (APCVD) following procedures reported previously.[21−23] The α-Fe_2O_3 films investigated here were typically ∼400−500 nm thick.

B. Electrodeposition of Co−Pi. For Co−Pi deposition onto α-Fe_2O_3 photoanodes, electrical tape with an aperture that matched the irradiated area during photoelectrochemical (PEC) experiments (ø = 6 mm diameter) was applied onto the α-Fe_2O_3. Co−Pi was then electrodeposited on the exposed area under the conditions communicated previously.[21] As the working electrode, α-Fe_2O_3 was submerged into a solution of 0.5 mM cobalt nitrate in 0.1 M pH 7 potassium phosphate (KPi) buffer. A Pt mesh was used as the counter electrode, and saturated Ag/AgCl was used as the reference electrode. Co−Pi was electrodeposited at +1.1 V vs Ag/AgCl for 15 or 30 min. Typical current densities during deposition were ∼20−200 μA/cm^2 (see Supporting Information). For electrolysis studies involving Co−Pi on FTO, Co−Pi was electrodeposited for 15 min using the above conditions and a mask of 1 cm × 1 cm.

C. Photoelectrochemical Experiments. Current−voltage characteristics were measured using an Eco Chemie μ-Autolab II potentiostat in a home-built three-electrode optical cell using Ag/AgCl as the reference electrode and a Pt wire as the counter electrode. Contact to the photoanodes was made by a titanium clasp attached to the exposed FTO surface at the top of the anode, while the lower portion containing the sample was submerged in the electrolyte. Measurements were performed in 1 M NaOH(aq) at pH 13.6, 0.1 M KPi buffered at pH 8, and 0.1 M NaCl(aq) buffered at pH 8 with 0.1 M KPi. Potentials are reported vs Ag/AgCl (measured) or RHE (obtained using the relationship $E_{RHE} = E_{Ag/AgCl} + 0.0591 \times pH + 0.1976$ V). Photocurrent densities were measured under 1 sun, AM 1.5 simulated sunlight using an Oriel 96000 solar simulator equipped with a 150 W Xe arc lamp and an Oriel 81094 filter. The photoanodes were masked to illuminate a circular area of 6 mm diameter. Power dependence measurements were performed using an Ag variable neutral density filter, Thorlabs NDC-50C-2M. Unless otherwise stated, all films were illuminated from the front side of the photoanode. Unless otherwise specified, all experiments were performed at room temperature in air atmosphere.

D. Oxygen Detection. The detection of O_2 was performed using a YSI 5000 dissolved oxygen meter equipped with a YSI 5010 self-stirring Clark-type probe in a three-neck flask with an optical window. Before use, the electrolyte (0.1 M KPi buffered at pH 8) was degassed and purged with argon gas. Measurements were conducted in argon in the same three-electrode configuration described for PEC experiments using the same light source. Again, the photoanodes were masked to illuminate a circular area of 6 mm in diameter. Consecutive measurements were taken at +1.0, 1.1, and 1.23 V vs RHE for 2 h at each potential. While the light was off between voltages (∼160 s), there was no increase and sometimes even a decrease in the O_2 level due to consumption by the Clark electrode.

III. Results and Analysis

A. Co−Pi/α-Fe_2O_3 Photoanode Performance under Frontside Illumination and Mild pH Conditions. We previously reported the PEC performance of Co−Pi/α-Fe_2O_3 composite photoanodes in 1 M NaOH electrolyte using backside illumination or illumination through the FTO substrate.[21] Backside illumination was more efficient than frontside illumination because of nonproductive absorption of photons by the Co−Pi catalyst layer, but the photocurrent densities obtained with this configuration were relatively low (<1 mA/cm^2). α-Fe_2O_3 prepared by the APCVD method gives ∼2× more photocurrent density when illuminated from the front side,[23] however, so optimization of the composite photoanodes for frontside illumination was an objective of the present study. To reduce photon absorption by the catalyst, Co−Pi deposition times were decreased from the original 1 h duration.

Additionally, the basic electrolyte (pH 13.6) used in our previous study is undesirable for practical applications, and demonstration of Co−Pi water oxidation driven by α-Fe_2O_3 at more neutral pH was also an objective of the present study. A gradual decrease in photocurrent density from α-Fe_2O_3 anodes alone was observed under continuous illumination in 0.1 M KPi electrolyte at pH 7 and +1.3 V vs RHE (see Supporting Information). We therefore chose to explore PEC measurements

(17) Kanan, M. W.; Surendranath, Y.; Nocera, D. G. *Chem. Soc. Rev.* **2009**, *38*, 109–114.
(18) Nocera, D. G. *Inorg. Chem.* **2009**, *48*, 10001–10017.
(19) Nocera, D. G. *ChemSusChem* **2009**, *2*, 387–390.
(20) Turner, J. *Nat. Mater.* **2009**, *7*, 770–771.
(21) Zhong, D. K.; Sun, J.; Inumaru, H.; Gamelin, D. R. *J. Am. Chem. Soc.* **2009**, *131*, 6086–6087.
(22) Kay, A.; Cesar, I.; Grätzel, M. *J. Am. Chem. Soc.* **2006**, *128*, 15714–15721.
(23) Cesar, I.; Sivula, K.; Kay, A.; Zboril, R.; Grätzel, M. *J. Phys. Chem. C* **2009**, *113*, 772–782.

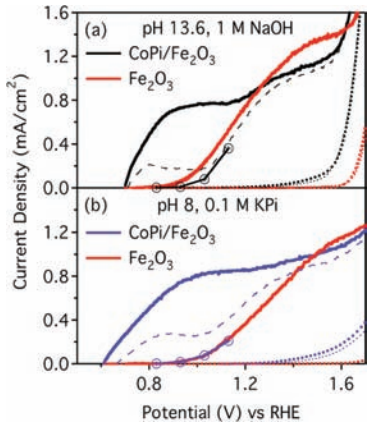

Figure 1. Dark current (dotted) and photocurrent (solid and dashed) densities of α-Fe_2O_3 photoanodes before and after 30 min of Co−Pi deposition, measured in pH 13.6 NaOH (a) and pH 8 KPi (b) at 50 (thick line) and 10 mV/s (dashed line). The α-Fe_2O_3 data (red curves) were collected at 10 mV/s. The circles denote steady-state photocurrent densities after 200 s of continuous illumination under 1 sun, AM 1.5 simulated sunlight.

in electrolytes at pH 8, which is around the pH of natural seawater.[24] Two approaches were used to achieve this pH. One involved use of 0.1 M potassium phosphate (KPi), the electrolyte used in most Co−Pi electrolysis experiments,[13,15] buffered to pH 8. The second involved 0.1 M NaCl buffered to pH 8 with 0.1 M KPi.

Figure 1 shows current−voltage ($J-V$) curves collected for Co−Pi/α-Fe_2O_3 composite photoanodes prepared with 30 min deposition of Co−Pi and measured in various electrolytes. Each data set is compared to analogous data collected for the same Fe_2O_3 film measured before Co−Pi deposition. Figure 1a shows the $J-V$ curves collected using 1 M NaOH at pH 13.6, and Figure 1b shows data collected using 0.1 M KPi at pH 8. As documented previously,[21] in 1 M NaOH, Co−Pi deposition yields a cathodic shift of >350 mV in the photocurrent onset potential relative to α-Fe_2O_3 (Figure 1a). PEC measurements in 0.1 M KPi electrolyte at pH 8 also show similar shifts. With frontside illumination there is only a slight decrease in the photocurrent density at high applied potentials (+1.3−1.6 V) compared to α-Fe_2O_3 alone, attributed to partial photon absorption by the catalyst layer. The data in Figure 1 demonstrate that Co−Pi/α-Fe_2O_3 composite photoanodes can operate under reduced pH conditions and with frontside illumination.

B. Kinetic Bottleneck in Co−Pi/α-Fe_2O_3 Composite Photoanodes. In the course of these efforts to optimize the Co−Pi/α-Fe_2O_3 composite photoanodes, it was recognized that improvements in efficiency were often accompanied by increasingly apparent symptoms[25] of kinetic limitations. For example, Figure 1 also shows $J-V$ curves of the same Co−Pi/α-Fe_2O_3 composite photoanodes measured at the slower scan rate of 10 mV/s (dashed line). The open circles in Figure 1 are the quasi-steady-state photocurrent densities measured after 200 s of simulated solar irradiation at each applied potential (vide infra). The cathodic shift and photocurrent densities both decrease as the scan rate is slowed, converging on those of the underlying α-Fe_2O_3 at the slowest scan rates. Upon increasing the scan rate again, the $J-V$ curves recover their original shape, even

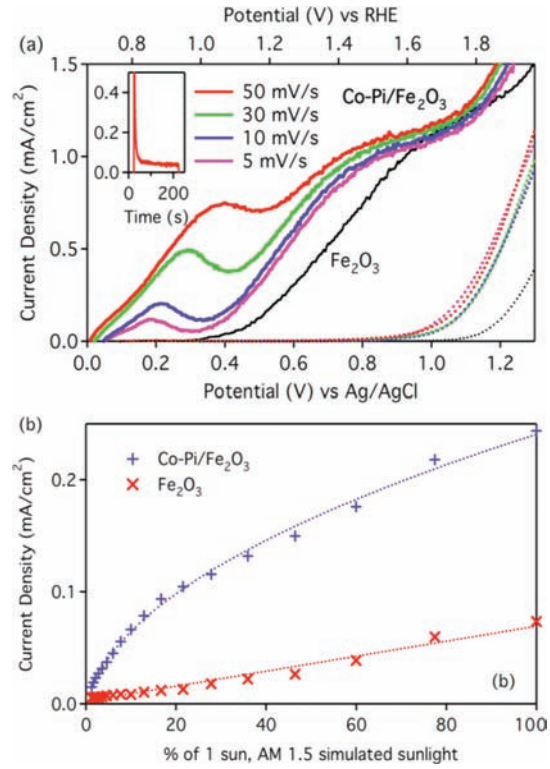

Figure 2. (a) Dark current (dotted) and photocurrent (solid) densities of an α-Fe_2O_3 photoanode before (thin black) and after 30 min of Co−Pi deposition (thick colored) in 0.1 M KPi electrolyte at pH 8. The α-Fe_2O_3 data (black curves) were collected at 10 mV/s. (Inset) Photocurrent density vs time at +1.1 V vs RHE. (b) Power dependence of photocurrent density for an α-Fe_2O_3 photoanode before (red) and after (blue) Co−Pi deposition, measured at +1.0 V vs RHE.

after 10+ h of continuous illumination. Illuminating with chopped light also recovers the photocurrent enhancement. This behavior is largely independent of electrolyte or pH (Figure 1) and suggests the existence of a kinetic bottleneck in the performance of these Co−Pi/α-Fe_2O_3 composite photoanodes.

To detail this kinetic bottleneck, its symptoms were explored in various complementary measurements on a single Co−Pi/α-Fe_2O_3 composite photoanode in 0.1 M KPi electrolyte at pH 8. The resulting data are summarized in Figure 2. Expanding on Figure 1, photocurrents were measured at a greater variety of scan rates to show the evolving characteristics of the $J-V$ curves. With faster scan rates, the first maximum shifts to higher potentials. The inset shows the photocurrent response vs time upon unblocking the light path, measured at +1.1 V vs RHE. A large initial spike in photocurrent upon illumination is followed by multiexponential decay to a lower steady-state current density with an effective time constant on the order of $\tau \approx 10$ s, i.e., comparable to the data collection time scale (tens of seconds). At least some of the initial current density in this trace can be attributed to cobalt oxidation, which is an essential step in the water oxidation mechanism.[19] Oxygen detection experiments in 0.1 M KPi at 1 V vs RHE show that this initial high current density is accompanied by a spike in the oxygen evolution rate, however, which then also decreases as the current density decays (see Supporting Information). The spike and subsequent current density decay therefore cannot be ascribed solely to an initial charging current for the redox active Co−Pi layer. Figure 2b plots the steady-state photocurrent density for a Co−Pi/α-Fe_2O_3 composite photoanode measured as a function

(24) Doney, S. C. *Sci. Am.* **2006**, *294*, 58–65.
(25) Bard, A. J.; Stratmann, M.; Licht, S. *Encyclopedia of Electrochemistry: Semiconductor Electrodes and Photoelectrochemistry*; Wiley-VCH: New York, 2002.

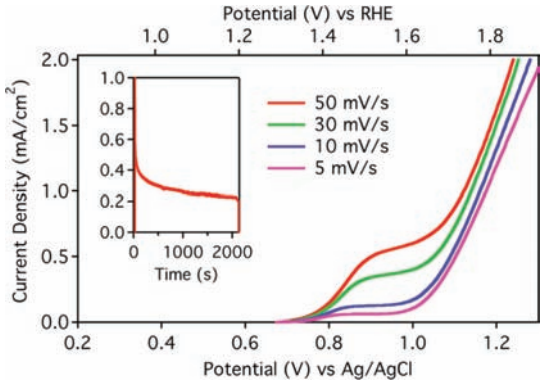

Figure 3. Linear sweep voltammetry of Co−Pi on FTO at various scan rates in pH 7, 0.1 M KPi electrolyte. (Inset) Decay of the bulk electrolysis current density over time under these conditions, measured at +1.1 V vs Ag/AgCl (+1.3 V vs NHE).

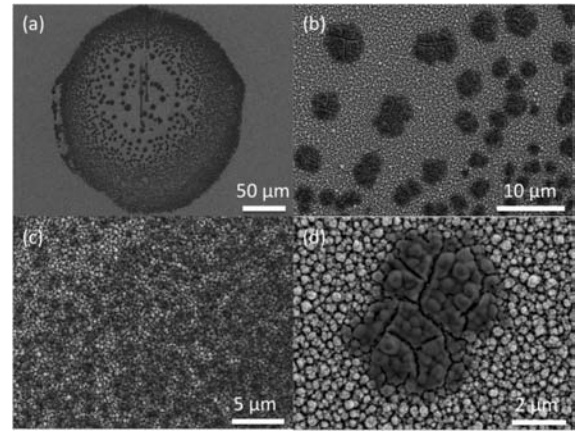

Figure 4. Scanning electron micrographs of Co−Pi/α-Fe_2O_3 composite photoanodes showing (a) ring-like deposition of Co−Pi in selective areas of the α-Fe_2O_3 surface and (b−d) magnified views of Co−Pi patches within this ring. (d) Co−Pi conforming to the topology of the underlying α-Fe_2O_3 mesostructure. The cracks in the Co−Pi result from drying.

of illumination power density between 0 and 1 sun. There is a marked saturation in the photocurrent as the light intensity is increased.

Overall, four major symptoms of this kinetic bottleneck can be identified: (i) a scan rate dependence, (ii) a kinetic decay in the photocurrent density, (iii) photocurrent saturation upon increased illumination, and (iv) a sweep-rate-dependent maximum at the beginning of the $J-V$ curve. The sweep-rate dependence of this maximum is a consequence of the superposition of an increasing current density from increasing bias with a current decay of the type illustrated in Figure 2(inset).

Parallel measurements were performed for α-Fe_2O_3 photoanodes alone under the same experimental conditions. Under the conditions represented in Figure 1, the $J-V$ curves of α-Fe_2O_3 photoanodes did not change significantly with scan rate (data collected at 10 mV/s are plotted in Figure 1). In time-dependence measurements, irradiation typically induced a small initial current spike followed by relaxation to a similar steady-state value within a few seconds. Finally, the α-Fe_2O_3 photocurrents increased much more linearly with increasing light intensity under these conditions (Figure 2b). These observations suggest that the kinetic bottleneck is likely associated with the Co−Pi modification, perhaps as an intrinsic limitation of the catalyst under these conditions or perhaps because of slow interfacial electron transfer.

To test the catalyst alone, Co−Pi was electrodeposited on FTO and electrochemical experiments were conducted in 0.1 M KPi electrolyte buffered to pH 7 with stirring. Figure 3 shows the $J-V$ characteristics of Co−Pi at various scan rates and the current density time dependence under typical electrolysis conditions of +1.1 V vs Ag/AgCl. Like in Figure 2, the bulk electrolysis by Co−Pi on FTO also shows a scan rate dependence and a decay in the current density in the region where water oxidation is normally observed, +1.3 V vs NHE or +1.7 V vs RHE. These observations confirm the hypothesis that the kinetic bottleneck observed in the Co−Pi/α-Fe_2O_3 photoanodes is associated with the Co−Pi catalyst itself rather than with the Co−Pi/α-Fe_2O_3 interface.

C. Alleviating the Kinetic Problem in Co−Pi/α-Fe_2O_3. If there is a kinetic bottleneck in Co−Pi/α-Fe_2O_3 photoanodes, we hypothesized that even further reduction of the Co−Pi deposition time may remediate the problem. For example, thick layers of Co−Pi may inhibit rapid charge or proton transport from electrolyte through the catalyst, thus restricting current flow and allowing other nonproductive recombination pathways to become competitive. To test this possibility, Co−Pi was electrodeposited on α-Fe_2O_3 photoanodes for only 15 min, one-half the initial deposition time and one-quarter of the time reported previously.[21] Figure 4 shows SEM images of the resulting Co−Pi/α-Fe_2O_3 composite photoanode. Unlike the dense coverage of Co−Pi on α-Fe_2O_3 after 1 h of electrodeposition described previously,[21] 15 min deposition results in only sparse coverage of the α-Fe_2O_3 photoanode by Co−Pi, which now displays ring-like patterns on the surface (Figure 4a). These ring patterns are formed from smaller patches of Co−Pi (Figure 4b−d). These patches are estimated to be ≪100 nm thick, compared to the ∼200 nm thick film that was deposited during 1 h deposition,[21] and show cracking due to drying. The Co−Pi layer conforms to the topology of the α-Fe_2O_3 so well that the microstructure of the α-Fe_2O_3 surface can still even be seen through the catalyst in places. We hypothesize that these patches are somehow associated with scratches or pinholes in the α-Fe_2O_3 that allow current to flow more readily during electrodeposition. Indeed, preliminary energy-dispersive X-ray analysis (EDAX) experiments demonstrate the existence of a very thin catalyst layer over the entire α-Fe_2O_3 surface, and we thus hypothesize that catalysis is also distributed over the entire surface. Experiments to clarify this issue are underway.

PEC measurements were performed on these thinly covered Co−Pi/α-Fe_2O_3 photoanodes, and the results are shown in Figure 5. Cathodic shifts of ∼180 mV are again observed, as are enhanced photocurrents across the entire potential range. Importantly, the $J-V$ curves measured in NaOH electrolytes no longer exhibit the marked scan rate dependence that was observed for the parallel set of photoanodes with greater Co−Pi coverage (Figure 1). With a thinner layer of Co−Pi, the enhanced current density is maintained even after 200 s (Figure 5) and the cathodic shift is stable. For PEC measurements conducted in 0.1 M KPi at pH 8, a gradual decay in the photocurrent over time was still evident and the cathodic shift decreased from ∼200 to 150 mV after 200 s of continuous illumination (Figure 5b). PEC measurements were also performed in 0.1 M NaCl buffered to pH 8 with KPi. Chloride has been shown previously not to interfere with Co−Pi catalysis at pH 7 in KPi.[14] The resulting $J-V$ curves with NaCl added are essentially indistinguishable from those without NaCl (Figure 5b), demonstrating that PEC water oxidation with Co−Pi/α-

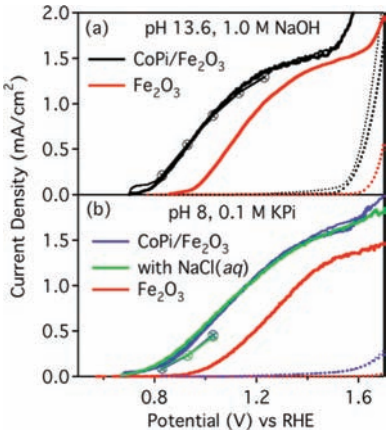

Figure 5. Dark current (dotted) and photocurrent (solid) densities of an α-Fe_2O_3 photoanode before (red) and after 15 min of Co−Pi deposition, measured in (a) pH 13.6 NaOH and (b) pH 8 KPi with (green) and without (blue) 0.1 M NaCl at 50 (thin line) and 10 mV/s (thick line). The α-Fe_2O_3 data (red curves) were collected at 10 mV/s. The circles denote steady-state photocurrent densities after 200 s of continuous illumination under 1 sun, AM 1.5 simulated sunlight.

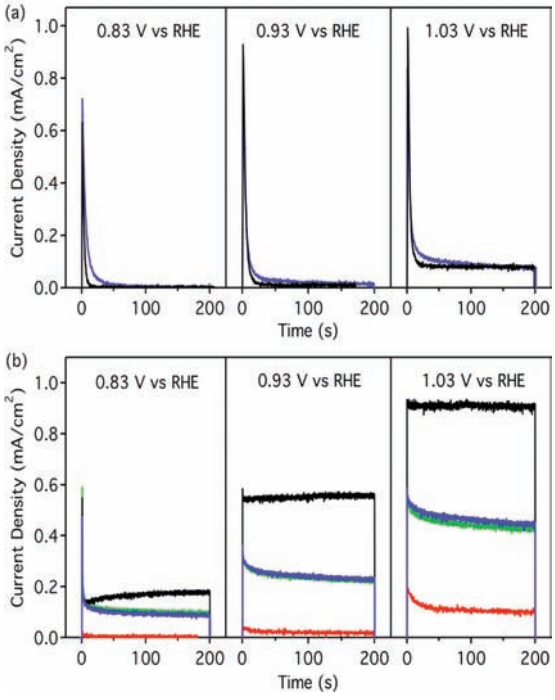

Figure 6. Photocurrent decay curves measured under 1 sun, AM 1.5 simulated sunlight at various applied potentials for Co−Pi/α-Fe_2O_3 composite photoanodes in pH 8 KPi (blue), pH 8 buffered salt water (green), and pH 13.6 NaOH (black) electrolytes. (a) Data collected following 30 min of Co−Pi deposition, and (b) data collected following 15 min of Co−Pi deposition. Photocurrent decay curves measured for α-Fe_2O_3 in pH 8, 0.1 M KPi electrolyte (red) are included in panel b for comparison.

Fe_2O_3 composite photoanodes can be performed equally well in the presence of chloride.

Figure 6 compares the kinetic responses of Co−Pi/α-Fe_2O_3 photoanodes with thicker (Figure 6a, 30 min deposition, see Supporting Information) and thinner (Figure 6b, 15 min deposition, Figure 4) Co−Pi coverage. The photocurrent decay curves of Figure 6a all show a large initial spike in current density followed by a multiexponential decrease with $\tau \approx 10$ s to a small steady-state photocurrent density close to that of the underlying α-Fe_2O_3 photoanode. In contrast, the photoanodes with thinner Co−Pi coverage all show substantially more stable performance. In all cases, the steady-state photocurrent densities in Figure 6b are enhanced relative to those of the parent α-Fe_2O_3 photoanodes (red curves). The result is a sustainable photocurrent density that is enhanced relative to α-Fe_2O_3 by more than an order of magnitude at 0.83 V, where α-Fe_2O_3 alone does not exhibit significant photocurrent (Figure 6b). Gains in photocurrent are less substantial at higher applied potentials, likely due to contributions directly from α-Fe_2O_3. Overall, the data in Figures 5 and 6 demonstrate that reduced Co−Pi deposition onto α-Fe_2O_3 photoanodes circumvents the major kinetic limitations identified above while still shifting the onset potential of α-Fe_2O_3 by ∼180 mV and simultaneously facilitates frontside illumination for maximum photocurrent densities.

Decreased deposition of Co−Pi onto α-Fe_2O_3 largely overcomes the kinetic limitations described in Figure 2, but there is still some evidence of such kinetic effects in KPi electrolyte (Figures 5b and 6b) that are completely absent in 1 M NaOH. For 1 M NaOH, there is a small initial spike in the photocurrent followed by a small gradual increase to steady state. A similar response has been observed previously in α-Fe_2O_3 at large applied potentials.[26] These observations suggest that the kinetic bottleneck may be related to diffusion of the proton acceptor under these experimental conditions. In the Co−Pi catalytic mechanism proposed in ref 17 a Co^{3+}−hydroxide intermediate undergoes proton-coupled electron transfer in which the proton is likely removed by the proton-accepting electrolyte. It is conceivable that limited mobility of protons through the amorphous catalyst may contribute to the kinetic bottleneck described by Figures 2−4 and that OH^- is better able to overcome this limitation. Overall, the data in Figures 5 and 6 show that this bottleneck is lessened by changing the electrolyte from pH 8 KPi to pH 13.6 NaOH and is effectively circumvented by reducing the density of catalyst on the α-Fe_2O_3 surface.

D. Oxygen Evolution. In addition to current density measurements, PEC O_2 evolution by the Co−Pi/α-Fe_2O_3 composite photoanodes was also examined. Oxygen evolution was measured at various applied potentials before and after 15 min of Co−Pi electrodeposition onto an α-Fe_2O_3 photoanode. Measurements were performed in 0.1 M KPi electrolyte at pH 8 to allow comparison with electrolysis results collected under similar conditions.[13] Figure 7a shows the $J-V$ characteristics of the α-Fe_2O_3 photoanode used for these measurements before and after Co−Pi deposition and for both front- and backside illumination. Photocurrent densities increased substantially with frontside illumination, particularly at low potentials. Figure 7b plots the photocurrent density vs time along with the O_2 concentrations measured simultaneously using the Clark-type electrode.

Sustained photocurrent was observed for the Co−Pi/α-Fe_2O_3 composite photoanode over the course of this ∼6 h experiment. This steady-state photocurrent was enhanced over that of the parent α-Fe_2O_3 film, even after several hours of illumination, and was accompanied by a correspondingly large enhancement in the O_2 evolution rate. The photocurrent density and O_2 evolution enhancement factors (J(Co−Pi/α-Fe_2O_3)/J(α-Fe_2O_3) and $\{d[O_2]/dt(\text{Co−Pi}/\alpha\text{-}Fe_2O_3)\}/\{d[O_2]/dt(\alpha\text{-}Fe_2O_3)\}$, respectively) measured at each applied potential are indicated in Figure 7b. The amount of dissolved O_2 detected by the Clark-type

(26) Eggleston, C. M.; Shankle, A. J. A.; Moyer, A. J.; Cesar, I.; Grätzel, M. *Aquat. Sci.* **2009**, *71*, 151–159.

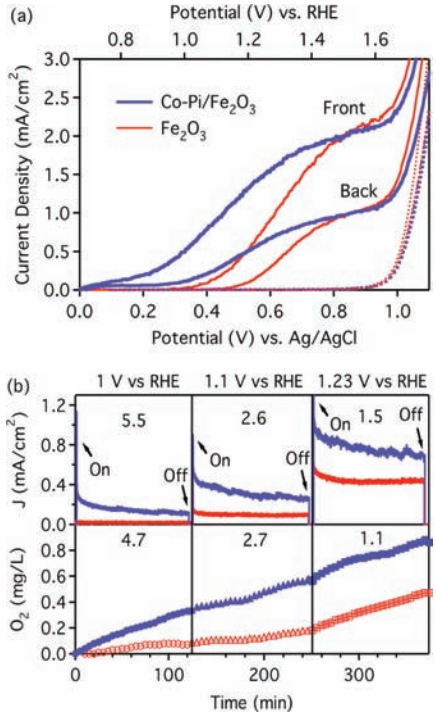

Figure 7. (a) Dark current (dotted) and photocurrent (solid) densities measured for an α-Fe_2O_3 photoanode before (red) and after (blue) 15 min of Co−Pi deposition. Data collected at 10 mV/s, for both front- and backside illumination. (b) Photocurrent density and O_2 generation measured for the above photoanodes vs time: Co−Pi/α-Fe_2O_3 (blue) and α-Fe_2O_3 (red). The numbers in b indicate the photocurrent and O_2 enhancement factors (see text). Bubbles adhering to and releasing from the photoanode surface cause disruptions in the current density. All PEC data were collected under 1 sun, AM 1.5 simulated solar irradiation.

electrode was lower than the theoretical maximum for the measured current densities, but this difference is attributable to the adherence of bubbles on the rough surface of the Co−Pi/α-Fe_2O_3 photoanode. Occasional jumps in the photocurrent density were observed for the composite photoanodes and are related to release of these bubbles.

The data in Figure 7b show that PEC O_2 evolution by the Co−Pi/α-Fe_2O_3 composite photoanode is enhanced over that of the same α-Fe_2O_3 photoanode without Co−Pi. Despite the gradual decline in photocurrent density for these photoanodes when measured in 0.1 M KPi electrolyte at pH 8 (Figures 5 and 6), after 2 h of continuous irradiation at +1.0 V vs RHE ~5 times more oxygen was produced for the Co−Pi-modified α-Fe_2O_3 photoanode with no detectable degradation in performance.

IV. Summary

The photoelectrochemical performance of Co−Pi/α-Fe_2O_3 composite photoanodes for water oxidation has been improved by optimization for frontside illumination in pH 8 electrolytes. A kinetic bottleneck was identified that appears to be related to the Co−Pi catalyst itself under these conditions. This kinetic bottleneck was overcome by more sparse deposition of Co−Pi onto α-Fe_2O_3. Following these improvements, sustained water oxidation by Co−Pi/α-Fe_2O_3 composite photoanodes was demonstrated in both photocurrent and O_2 evolution measurements. Photoelectrochemical water oxidation by the Co−Pi/α-Fe_2O_3 composite photoanodes was enhanced relative to that of α-Fe_2O_3 alone: Under these conditions, a 5-fold enhancement in the photocurrent density and water oxidation rate was

Scheme 1

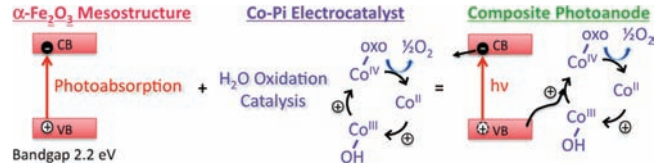

observed at +1.0 V vs RHE. This enhancement is even more substantial at <1.0 V vs RHE, where α-Fe_2O_3 alone does not exhibit significant photocurrent at all.

It is also interesting to compare these results with those obtained for bulk electrolysis by Co−Pi without a photon-absorbing substrate. By itself, Co−Pi electrolysis current densities reach ~1.2 mA/cm^2 at an applied bias of +1.29 V vs NHE (pH 7)[13] or ~+1.7 V vs RHE. In conjunction with an inexpensive and robust photoanode such as α-Fe_2O_3 under 1 sun, AM 1.5 illumination, the applied bias necessary to achieve the same current density can be reduced by over 0.5 V in buffered salt water at pH 8, the average pH of seawater.[24] The results described here thus demonstrate that sustained O_2 evolution in mild salt water conditions can be achieved with significantly reduced external power demands relative to Co−Pi alone, albeit in the low current density regime, by integrating this catalyst with a light-harvesting semiconductor substrate. The overall process, in which photogenerated holes in α-Fe_2O_3 are converted to oxidizing equivalents in Co−Pi, yielding O_2 evolution well below the Co−Pi bulk electrolysis threshold potential, is summarized schematically in Scheme 1. Further improvement of the performance of these composite photoanodes can be anticipated, for example, by variation of the Co−Pi deposition conditions to optimize photocurrent densities at extremely low bias. More generally, these results emphasize that composite photoanode strategies offer promising prospects for sustainable, affordable, and distributed solar fuel technologies and warrant efforts to extend this strategy to include other catalysts such as IrO_2,[27,28] Mn−oxo complexes,[29,30] or $[Ru(L)_2(OH_2)]^{2+}$ complexes,[31] which can be powered in part or entirely by light-harvesting electrodes.

Acknowledgment. The authors thank Dr. Jianwei Sun and Dr. Steve Reece for valuable discussions. This work was funded by the ACS-PRF (AC), the NSF (IGERT, DGE-050-4573), the University of Washington, and the UW Initiative Fund (UIF) and was partially conducted at the UW Nanotechnology User Facility, a member of NNIN.

Supporting Information Available: Additional photocurrent decay, electrodeposition, oxygen evolution, and SEM data. This material is available free of charge via the Internet at http://pubs.acs.org.

JA908730H

(27) Youngblood, W. J.; Lee, S.-H. A.; Maeda, K.; Mallouk, T. E. *Acc. Chem. Res.* **2009**, *42*, 1966–1973.
(28) Nakagawa, T.; Bjorge, N. S.; Murray, R. W. *J. Am. Chem. Soc.* **2009**, *131*, 15578–15589.
(29) Li, G.; Sproviero, E. M.; McNamara, W. R.; Snoeberger, R. C.; Crabtree, R. H.; Brudvig, G. W.; Batista, V. S. *J. Phys. Chem. B* **2009**, ASAP (10.1021/jp908925z).
(30) Dismukes, G. C.; Brimblecombe, R.; Gelton, G. A. N.; Pryadun, R. S.; Sheats, J. E.; Spiccia, L.; Swiegers, G. F. *Acc. Chem. Res.* **2009**, *42*, 1935–1943.
(31) Chen, Z.; Concepcion, J. J.; Jurss, J. W.; Meyer, T. J. *J. Am. Chem. Soc.* **2009**, *131*, 15580–15581.